Nonlinear dynamo mode dynamics in reversed field pinches

Richard Fitzpatrick and Edmund P. Yu

Articles you may be interested in

Mode- and plasma rotation in a resistive shell reversed-field pinch
Phys. Plasmas **11**, 647 (2004); 10.1063/1.1639016

Evolution process of the mode wall-locking and phase-locking in a reversed-field pinch plasma
Phys. Plasmas **8**, 1625 (2001); 10.1063/1.1364674

Effect of a resistive vacuum vessel on dynamo mode rotation in reversed field pinches
Phys. Plasmas **6**, 3878 (1999); 10.1063/1.873650

Stability of resistive wall modes in reversed field pinches with longitudinal flow and dissipative effects
Phys. Plasmas **6**, 3868 (1999); 10.1063/1.873191

Feedback stabilization of resistive shell modes in a reversed field pinch
Phys. Plasmas **6**, 3536 (1999); 10.1063/1.873614

Nonlinear dynamo mode dynamics in reversed field pinches*

Richard Fitzpatrick and Edmund P. Yu
Institute for Fusion Studies, Department of Physics, University of Texas at Austin, Austin, Texas 78712

The nonlinear dynamics of a typical dynamo mode in a reversed field pinch, under the action of the braking torque due to eddy currents excited in a resistive vacuum vessel and the locking torque due to a resonant error-field, is investigated. A simple set of phase evolution equations for the mode is derived: these equations represent an important extension of the well-known equations of Zohm *et al.* [Europhys. Lett. **11**, 745 (1990)] which incorporate a self-consistent calculation of the radial extent of the region of the plasma which corotates with the mode; the width of this region being determined by plasma viscosity. Using these newly developed equations, a comprehensive theory of the influence of a resistive vacuum vessel on error-field locking and unlocking thresholds is developed. Under certain circumstances, a resistive vacuum vessel is found to strongly *catalyze* locked mode formation. Hopefully, the results obtained in this paper will allow experimentalists to achieve a full understanding of why the so-called ''slinky mode'' locks in some reversed field pinch devices, but not in others. The locking of the slinky mode is currently an issue of outstanding importance in reversed field pinch research. © *2000 American Institute of Physics.* [S1070-664X(00)01309-4]

I. INTRODUCTION

A reversed field pinch (or RFP) is a magnetic fusion device in which a thermonuclear plasma is confined via a combination of a toroidal magnetic field, B_ϕ, and a poloidal magnetic field, B_θ, in an axisymmetric toroidal configuration.[1] The RFP concept derives its name from the fact that the toroidal magnetic field spontaneously reverses direction in the outer regions of the plasma. This reversal is a consequence of relaxation to a minimum energy state driven by intense magnetohydrodynamical (MHD) mode activity during the plasma start-up phase.[2] Intermittent, relatively low-level, mode activity maintains the reversal, by dynamo action, throughout the duration of the plasma discharge.

A conventional RFP plasma is surrounded by a thick conducting shell whose resistive penetration time is much longer than the duration of the discharge. Such a shell is necessary in order to stabilize external kink modes which would otherwise rapidly destroy the plasma.[3] In the presence of the shell, the dominant MHD modes are $m=1$ tearing modes resonant in the plasma core. These modes possess a range of toroidal mode numbers, characterized by $n \sim 2 R_0/a$. Here, m,n are poloidal and toroidal mode numbers, respectively, whereas a and R_0 are the minor and major radii of the plasma, respectively. The core tearing modes are responsible for the dynamo action which maintains the field reversal, and are, therefore, generally known as *dynamo modes*.[4]

The majority of RFP experiments [e.g., the Reversed Field Experiment (RFX) (Ref. 5), and the TPE-RX (Ref. 6) experiment] also feature a thin resistive vacuum vessel situ-

ated between the edge of the plasma and the stabilizing shell.

The key to the success of the RFP concept lies in the *control* of MHD instabilities; there is clear experimental evidence that a relatively modest reduction in ambient mode amplitudes leads to a dramatic improvement in plasma confinement.[7] However, in order to reliably control dynamo modes in RFPs, it is first necessary to fully *understand* their dynamics.

The complex nonlinear dynamics of dynamo modes in RFPs is a fascinating subject in its own right, as well as a topic of great practical importance. Dynamo modes in RFPs are generally observed to *phase lock* to one another, at relatively low amplitudes, so as to form a *toroidally localized* structure in the perturbed magnetic field known as a ''slinky mode.''[8,9] This effect can be understood as a natural consequence of the mutual nonlinear couplings of the various modes in the plasma.[10] The slinky mode per se does *not* appear to significantly degrade the global plasma confinement.[11] Instead, it gives rise to a toroidally localized ''hot spot'' on the plasma facing surface, presumably because the radial transport due to the diffusion of chaotic magnetic field-lines peaks at the toroidal angle where the amplitude of the slinky mode attains its maximum value. The hot spot is not a problem as long as the slinky mode *rotates* in the laboratory frame. Conversely, if, for some reason, the slinky mode ceases to rotate then the hot spot is forced to hover over the same point on the plasma facing surface, leading almost inevitably to overheating, the influx of impurities into the plasma, and the premature termination of the discharge. The enhanced plasma–wall interaction associated with a locked slinky mode is of major concern to fusion researchers, since it is a limiting factor in virtually all current RFP experiments.[12,13] Recent experiments on RFX have demonstrated that this problem can be alleviated, to some extent, by *forcing* the locked slinky mode to rotate via the

imposition of a propagating ripple pattern onto the equilibrium toroidal magnetic field.[14] These experiments seem to confirm the idea that the slinky mode is only a major problem when it fails to rotate.

The physical mechanisms which are most likely to be responsible for converting slinky modes, and their constituent dynamo modes, from rotating modes (their natural state) to locked modes in RFPs are ''error-fields'' and eddy currents excited in the resistive vacuum vessel. Error-fields are small nonaxisymmetric perturbations in the equilibrium magnetic field generated by field–coil misalignments, current feeds, and the presence of insulating gaps in the conducting shell. The ability of those helical components of error-fields which *resonate* with the plasma core to arrest dynamo mode rotation in RFPs is well-known[15–17] and well understood.[18] However, it was recently pointed out that the eddy currents excited in the resistive vacuum vessels of present-day RFPs by rotating dynamo modes exert slowing-down torques on these modes which are generally sufficiently strong to reduce their rotation to *extremely* low levels.[19] Of course, eddy current torques cannot, by themselves, completely halt the rotation of a dynamo mode, since there is zero torque when the mode is stationary. It is concluded, therefore, that the locking of dynamo modes (and, hence, of slinky modes) in RFPs is most probably a *combined* effect of resonant error-fields and eddy currents excited in the resistive vacuum vessel.

The aim of this paper is to develop a theoretical framework within which the *phase evolution* of rotating dynamo modes in RFPs, in the presence of resonant error-fields and a thin resistive shell surrounding the plasma, can be analyzed. In particular, it is hoped to develop a set of phase evolution equations which are sufficiently simple that experimentalists can routinely employ them whilst interpreting data or designing new RFP experiments.

The model adopted in this paper is somewhat simplistic. Instead of considering a range of unstable $m=1$ modes, it focuses on the dynamics of a *single* representative dynamo mode in the presence of a resonant error-field and a thin resistive vacuum vessel surrounded by a thick conducting shell. Furthermore, the model only deals with zero-β, large aspect-ratio plasmas. Nevertheless, our model is probably sufficiently realistic to allow some progress to be made in our current understanding of locked mode formation in RFPs.

II. PRELIMINARY ANALYSIS

A. The plasma equilibrium

Consider a large aspect-ratio,[20] zero-β,[21] RFP plasma equilibrium whose unperturbed magnetic flux-surfaces map out (almost) concentric circles in the poloidal plane. Such an equilibrium is well approximated as a periodic cylinder. Suppose that the minor radius of the plasma is a. Standard cylindrical polar coordinates (r,θ,z) are adopted. The system is assumed to be periodic in the z-direction, with periodicity length $2\pi R_0$, where R_0 is the simulated major radius of the plasma. It is convenient to define a simulated toroidal angle $\phi=z/R_0$.

The equilibrium magnetic field is written $\mathbf{B}=[0,B_\theta(r),B_\phi(r)]$, where $\nabla\wedge\mathbf{B}=\sigma(r)\mathbf{B}$.

B. Outline of the problem

Suppose that the plasma (minor radius a) is surrounded by a concentric, thin, resistive shell of minor radius b. The resistive shell is, in turn, surrounded by a concentric, perfectly conducting shell of minor radius c. It follows that $a<b<c$. The conducting shell is assumed to contain thin vacuum gaps though which a static, externally generated, nonaxisymmetric error-field can leak. This paper investigates the effect of such an error-field, and any helical eddy currents excited in the resistive shell, on the rotation of a typical core tearing mode; the m,n mode, say. All other modes in the plasma are ignored, for the sake of simplicity.

C. The perturbed magnetic field

The magnetic perturbation associated with the m,n tearing mode can be written

$$\mathbf{b}(\mathbf{r},t)=\mathbf{b}^{m,n}(r,t)e^{i(m\theta-n\phi)}. \tag{1}$$

In this paper, it is assumed that $m>0$ and $n\neq0$. The linearized magnetic flux function $\psi^{m,n}(r,t)\equiv-irb_r^{m,n}$ satisfies Newcomb's equation,[22]

$$\frac{d}{dr}\left[f^{m,n}\frac{d\psi^{m,n}}{dr}\right]-g^{m,n}\psi^{m,n}=0, \tag{2}$$

where

$$f^{m,n}(r)=\frac{r}{m^2+n^2\epsilon^2}, \tag{3}$$

$$g^{m,n}(r)=\frac{1}{r}+\frac{r(n\epsilon B_\theta+mB_\phi)}{(m^2+n^2\epsilon^2)(mB_\theta-n\epsilon B_\phi)}\frac{d\sigma}{dr}$$
$$+\frac{2mn\epsilon\sigma}{(m^2+n^2\epsilon^2)^2}-\frac{r\sigma^2}{m^2+n^2\epsilon^2}, \tag{4}$$

and $\epsilon=r/R_0$. As is well-known, Eq. (2) is *singular* at the m/n rational surface, minor radius r_s, which satisfies $F^{m,n}(r_s)=0$, where

$$F^{m,n}(r)\equiv mB_\theta(r)-n\epsilon(r)B_\phi(r). \tag{5}$$

In the vacuum region ($\sigma=0$) surrounding the plasma, the most general solution to Newcomb's equation takes the form

$$\psi^{m,n}=Ai_m(n\epsilon)+Bk_m(n\epsilon), \tag{6}$$

where A, B are arbitrary constants, and

$$i_m(n\epsilon)=|n\epsilon|I_{m+1}(|n\epsilon|)+mI_m(|n\epsilon|), \tag{7}$$

$$k_m(n\epsilon)=-|n\epsilon|K_{m+1}(|n\epsilon|)+mK_m(|n\epsilon|). \tag{8}$$

Here, I_m, K_m represent standard modified Bessel functions.

D. Standard tearing eigenfunctions

Let $\hat{\psi}_s^{m,n}(r,d)$ represent the normalized m,n tearing eigenfunction calculated assuming the presence of a single, perfectly conducting shell located at minor radius d. In other

words, $\hat{\psi}_s^{m,n}(r,d)$ is a *real* solution to Newcomb's equation (2) which is well behaved as $r \to 0$, and satisfies

$$\hat{\psi}_s^{m,n}(r_s,d)=1, \tag{9}$$

$$\hat{\psi}_s^{m,n}(d,d)=0. \tag{10}$$

It is easily demonstrated that $\hat{\psi}_s^{m,n}(r,d)$ is zero in the region $r > d$. In general, $\hat{\psi}_s^{m,n}(r,d)$ possesses gradient discontinuities at $r = r_s$ and $r = d$. The real quantity

$$E^{m,n}(d)=\left[r\frac{d\hat{\psi}_s^{m,n}(r,d)}{dr}\right]_{r_{s-}}^{r_{s+}} \tag{11}$$

can be identified as the standard m,n tearing stability index,[23] calculated assuming the presence of a single, perfectly conducting shell at a minor radius d.

E. Asymptotic matching

The quantity

$$\Psi_s^{m,n}(t)\equiv\psi^{m,n}(r_s,t) \tag{12}$$

represents the *reconnected magnetic flux* at the m,n rational surface. Likewise,

$$\Delta\Psi_s^{m,n}(t)\equiv\left[r\frac{d\psi^{m,n}}{dr}\right]_{r_{s-}}^{r_{s+}} \tag{13}$$

is a measure of the m,n helical current flowing in the vicinity of the rational surface. Note that both $\Psi_s^{m,n}$ and $\Delta\Psi_s^{m,n}$ are complex quantities.

Suppose that, in the absence of plasma and the perfectly conducting shell, the externally generated, static error-field is characterized by a magnetic flux function $\psi_{\text{ext}}(r,\theta,\phi)$. The perfectly conducting shell (minor radius c) is assumed to possess *narrow* gaps which allow the error-field to penetrate into the plasma. The m,n component of the error-field filtering through these gaps is characterized by

$$\Psi_c^{m,n}=\int\int_{\text{gaps}}\psi_{\text{ext}}(c,\theta,\phi)e^{-i(m\theta-n\phi)}\frac{d\theta}{2\pi}\frac{d\phi}{2\pi}, \tag{14}$$

where the integral is taken over the angular extent of the gaps.[10] Note that $\Psi_c^{m,n}$ is also a complex quantity.

Let

$$\Psi_s^{m,n}(t)=\hat{\Psi}_s e^{i\varphi_s(t)}, \tag{15}$$

$$\Psi_c^{m,n}=\hat{\Psi}_c e^{i\varphi_c}, \tag{16}$$

where $\hat{\Psi}_s$ and $\hat{\Psi}_c$ are both real. Now, φ_c is a constant for a *static* error-field. However,

$$\frac{d\varphi_s}{dt}=n\Omega_s(t), \tag{17}$$

where Ω_s is the plasma toroidal angular velocity at the m,n rational surface. This result follows since, according to standard MHD theory,[24] the m,n tearing mode is convected by the plasma at its own rational surface. The above constraint

is conventionally known as the "no slip" condition. In this paper, it is assumed that the plasma rotates *only* in the toroidal direction, for the sake of simplicity.

Standard asymptotic matching[19] across the rational surface and the resistive shell yields

$$\Delta\Psi_s^{m,n}=\left\{E^{m,n}(b)+\frac{[E^{m,n}(c)-E^{m,n}(b)]}{1+i\lambda^{m,n}}\right\}\Psi_s^{m,n}+E_{sc}^{m,n}\Psi_c^{m,n}, \tag{18}$$

where

$$\lambda^{m,n}=n\Omega_s\tau_b\frac{[E^{m,n}(c)-E^{m,n}(b)]}{E_{sb}^{m,n}E_{bs}^{m,n}}. \tag{19}$$

Here, τ_b is the *time constant* of the resistive shell, whose response is analyzed using the well-known "thin shell" approximation.[19] Furthermore,

$$E_{bs}^{m,n}=\frac{\hat{\psi}_s^{m,n}(a,b)(m^2+n^2\epsilon_b^2)}{k_m(n\epsilon_b)i_m(n\epsilon_a)-k_m(n\epsilon_a)i_m(n\epsilon_b)}, \tag{20}$$

$$E_{sb}^{m,n}=\frac{\hat{\psi}_s^{m,n}(a,b)(m^2+n^2\epsilon_s^2)}{k_m(n\epsilon_b)i_m(n\epsilon_a)-k_m(n\epsilon_a)i_m(n\epsilon_b)}, \tag{21}$$

$$E_{sc}^{m,n}=\frac{\hat{\psi}_s^{m,n}(a,c)(m^2+n^2\epsilon_s^2)}{k_m(n\epsilon_c)i_m(n\epsilon_a)-k_m(n\epsilon_a)i_m(n\epsilon_c)}, \tag{22}$$

where $\epsilon_s=r_s/R_0$, $\epsilon_a=a/R_0$, $\epsilon_b=b/R_0$, and $\epsilon_c=c/R_0$. Note that, under normal circumstances, $E^{m,n}(c)-E^{m,n}(b)$, $E_{bs}^{m,n}$, $E_{sb}^{m,n}$, and $E_{sc}^{m,n}$ are all positive quantities.

F. Electromagnetic torques

The toroidal electromagnetic torque acting in the vicinity of the m,n rational surface is given by[18]

$$\delta T_{\phi\text{EM}}^{m,n}=\frac{2\pi^2R_0}{\mu_0}\frac{n}{m^2+n^2\epsilon_s^2}\text{Im}\{\Delta\Psi_s^{m,n}(\Psi_s^{m,n})^*\}. \tag{23}$$

It follows from Eq. (18) that

$$\delta T_{\phi\text{EM}}^{m,n}=-\frac{2\pi^2R_0}{\mu_0}\frac{n}{m^2+n^2\epsilon_s^2}$$
$$\times\left\{\frac{\lambda^{m,n}[E^{m,n}(c)-E^{m,n}(b)]\hat{\Psi}_s^2}{1+(\lambda^{m,n})^2}\right.$$
$$\left.+E_{sc}^{m,n}\sin(\varphi_s-\varphi_c)\hat{\Psi}_s\hat{\Psi}_c\right\}. \tag{24}$$

Here, the first term on the right-hand side represents the braking torque due to eddy currents excited in the resistive shell, whereas the second term represents the locking torque due to the error-field. Incidentally, the electromagnetic torque exerted on the plasma by resistive shell eddy currents and the error-field is *localized* in the vicinity of the rational surface because of a standard result in MHD theory: namely, that net electromagnetic torques can only develop in those regions of a plasma in which (inertia-free) ideal-MHD breaks down (e.g., close to a rational surface).[24]

G. Plasma rotation

Let $\Omega(r)$ represent the toroidal angular velocity profile of the plasma. Likewise, $\Omega^{(0)}(r)$ represents the unperturbed velocity profile (i.e., the profile in the absence of resistive shell eddy currents and the resonant error-field). Finally, let

$$\Omega(r,t)=\Omega^{(0)}(r)+\Delta\Omega(r,t), \tag{25}$$

where $\Delta\Omega$ represents the *modification* to the plasma velocity profile induced by the eddy currents and the error-field.

The perturbed angular equation of motion of the plasma can be written

$$r\rho\frac{\partial\Delta\Omega}{\partial t}-\frac{\partial}{\partial r}\left(r\mu\frac{\partial\Delta\Omega}{\partial r}\right)=\frac{\delta T^{m,n}_{\phi\mathrm{EM}}}{4\pi^2 R_0^3}\delta(r-r_s), \tag{26}$$

where $\rho(r)$ is the plasma mass density profile, and $\mu(r)$ is the plasma (anomalous) perpendicular viscosity profile. Here, the radial extent of the nonideal region, centered on the rational surface, in which the electromagnetic torque develops is assumed to be negligible, for the sake of simplicity.

The boundary conditions which must be satisfied by the perturbed velocity profile are

$$\frac{\partial\Delta\Omega(0,t)}{\partial r}=0, \tag{27}$$

$$\Delta\Omega(a,t)=0. \tag{28}$$

The second boundary condition implies that the edge plasma velocity is essentially *unaffected* by the electromagnetic torque which develops in the vicinity of the rational surface. The assumptions underlying the analysis in this section are described in more detail in Ref. 24.

The *no slip* condition (17) can be rewritten

$$\frac{1}{n}\frac{d\varphi_s}{dt}=\Omega_s(t)=\Omega_s^{(0)}+\Delta\Omega(r_s,t), \tag{29}$$

where $\Omega_s^{(0)}=\Omega^{(0)}(r_s)$.

H. Normalization

Equations (24), (26), (27), (28), and (29) form a complete set which describe the phase evolution of a typical dynamo mode in a RFP under the influence of a resonant error-field and eddy currents excited in the resistive shell. It is now convenient to rewrite this set of equations in normalized form.

Let $\tilde{\Psi}_s=\hat{\Psi}_s/(r_s^2 F_s')$, $\tilde{\Psi}_c=\hat{\Psi}_c/(r_s^2 F_s')$, $\hat{r}=r/r_s$, $\hat{a}=a/r_s$, $\hat{\rho}=\rho/\rho(r_s)$, $\hat{\mu}=\mu/\mu(r_s)$, $\hat{t}=n\Omega_s^{(0)}t$, $\hat{\Omega}=\Omega/\Omega_s^{(0)}$, $\hat{\Omega}_s=\Omega_s/\Omega_s^{(0)}$, $\Delta\hat{\Omega}=\Delta\Omega/\Omega_s^{(0)}$, where $F_s'=(dF^{m,n}/dr)_{r_s}$. The typical hydromagnetic and viscous diffusion time scales can be written

$$\tau_H=\frac{\sqrt{\mu_0\rho(r_s)}}{F_s'}, \tag{30}$$

$$\tau_V=\frac{r_s^2\rho(r_s)}{\mu(r_s)}, \tag{31}$$

respectively.

Let

$$a_s=\frac{\tilde{\Psi}_s}{\Lambda_0}, \tag{32}$$

$$a_c=\frac{E_{sc}^{m,n}}{4[E^{m,n}(c)-E^{m,n}(b)]}\frac{\sqrt{v_l}}{v_s}\frac{\tilde{\Psi}_c}{\Lambda_0}, \tag{33}$$

$$v_s=\frac{E_{sb}^{m,n}E_{bs}^{m,n}}{n\Omega_s^{(0)}\tau_b[E^{m,n}(c)-E^{m,n}(b)]}, \tag{34}$$

$$v_l=\frac{1}{4n\Omega_s^{(0)}\tau_V(\int_1^{\hat{a}}d\hat{r}/\hat{r}\hat{\mu})^2}, \tag{35}$$

$$\Lambda_0=\left[\frac{(n\Omega_s^{(0)}\tau_H)^2\tau_b}{\tau_V}\frac{1}{2}\frac{m^2+n^2\epsilon_s^2}{n^2\epsilon_s^2}\frac{1}{E_{sb}^{m,n}E_{bs}^{m,n}}\middle/\int_1^{\hat{a}}\frac{d\hat{r}}{\hat{r}\hat{\mu}}\right]^{1/2}. \tag{36}$$

Here, a_s is the normalized dynamo mode amplitude, a_c is the normalized amplitude of the error-field, v_s is the critical normalized mode rotation velocity above which the resistive shell starts to act like a perfect conductor, v_l is the critical normalized mode rotation velocity above which the oscillating component of the plasma velocity profile, driven by the error-field, becomes localized around the rational surface, and Λ_0 is a convenient scale amplitude. Under normal circumstances, the parameters a_s and a_c are $O(1)$, whereas v_s, v_l, and Λ_0 are expected to be much less than unity.

The normalized phase evolution equations take the form

$$\frac{\hat{r}\hat{\rho}}{4J^2 v_l}\frac{\partial\Delta\hat{\Omega}}{\partial\hat{t}}-\frac{\partial}{\partial\hat{r}}\left(\hat{r}\hat{\mu}\frac{\partial\Delta\hat{\Omega}}{\partial\hat{r}}\right)=-\frac{\hat{T}}{J}\delta(\hat{r}-1), \tag{37}$$

$$\hat{T}=\frac{a_s^2}{4}\frac{\hat{\Omega}_s}{v_s^2+\hat{\Omega}_s^2}+\frac{a_s a_c}{\sqrt{v_l}}\sin(\varphi_s-\varphi_c), \tag{38}$$

$$\frac{\partial\Delta\hat{\Omega}(0,\hat{t})}{\partial\hat{r}}=0, \tag{39}$$

$$\Delta\hat{\Omega}(\hat{a},\hat{t})=0, \tag{40}$$

$$\frac{d\varphi_s}{d\hat{t}}\equiv\hat{\Omega}_s=1+\Delta\hat{\Omega}(1,\hat{t}), \tag{41}$$

where $J=\int_1^{\hat{a}}d\hat{r}/\hat{r}\hat{\mu}$. Equation (37) is the normalized equation of motion of the perturbed plasma rotation profile driven by the electromagnetic torque exerted at the rational surface. Equation (38) specifies the nature of this torque; it is the sum of contributions from eddy currents excited in the resistive shell and the resonant error-field, respectively. Equations (39) and (40) represent the boundary conditions which must be satisfied by the solution of Eq. (37). Finally, Eq. (41) is the *no slip* constraint, which relates the phase evolution of the dynamo mode to the plasma rotation velocity at its rational surface.

I. Discussion

This is an appropriate point at which to highlight the major assumptions made during the derivation of Eqs. (37)–(41), and also to discuss the relationship between this paper and previously published theoretical research on mode locking effects in magnetic fusion experiments.

The key assumptions made during the derivation of Eqs. (37)–(41) are as follows:

(1) The m,n dynamo mode is assumed to be *convected* by the plasma at its own rational surface. Furthermore, the electromagnetic torques exerted on the plasma by eddy currents excited in the resistive shell and the resonant error-field are assumed to be *localized* in the vicinity of the rational surface. Both of these results follow immediately from standard MHD theory, provided that the response of the plasma can be modeled according to linearized, inertia-free, ideal-MHD everywhere apart from a narrow region centered on the rational surface. For the typical mode amplitudes (between dynamo events), plasma densities and temperatures, and plasma rotation velocities observed in present-day RFPs, this approach is perfectly reasonable.

(2) The plasma in the vicinity of the m,n rational surface, which co-rotates with the mode, is assumed to be *strongly coupled* to the rest of the plasma via (anomalous) perpendicular viscosity. This assumption is certainly justified, given the typical momentum confinement time-scales observed in present-day RFPs.[25] The opposite approach, in which the plasma in the vicinity of the rational surface is assumed to be free to slip with respect to the bulk plasma,[26,27] would appear to be somewhat unphysical. The only possible exception to this rule occurs when the torque acting on the mode varies very rapidly in time (e.g., when the mode amplitude grows explosively[28]).

(3) It is assumed that the edge plasma rotation profile is determined by the balance of torques which are far larger in magnitude than those which typically develop in the plasma due to error-field or resistive shell eddy current effects. It follows that the edge plasma rotation is unlikely to be substantially affected by either error-field or eddy current torques; i.e., the plasma rotation profile acts like it is ''*clamped*'' at the edge. This assumption is justified theoretically in Ref. 24. It also seems to be in accordance with experimental observations [see, for instance, Fig. 4 in Ref. 29 and Fig. 4(a) in Ref. 30]. The opposite approach, in which the rotation profile is assumed to be subject to ''free slip'' boundary conditions at the plasma edge,[31] is difficult to justify on physical grounds.

(4) The amplitude evolution of the m,n mode is assumed to take place on a much slower time-scale than its phase evolution, and is, therefore, neglected in this paper. In other words, the amplitude evolution of dynamo modes is assumed *not* to play a *direct* role in their locking or unlocking to resonant error-fields or the resistive shell. This assumption is reasonable, given the typical mode rotation velocities and resistive growth-rates (between dynamo events) observed in present-day RFPs. In Ref. 24 it was found that the periodic modulation in the width of a magnetic island chain, as it rotates past a static error-field in a tokamak, can give rise to a significant, nonoscillating locking torque acting on that chain. It is easily demonstrated that this effect is negligible in present-day RFPs (because of the far larger saturated tearing mode amplitudes prevalent in RFPs compared to tokamaks).

(5) Any poloidal rotation of the plasma is neglected. This assumption is made mostly for convenience (it may actually be justified if RFP plasmas are subject to strong poloidal flow damping[32]), and could fairly easily be relaxed.

Many previously published papers have studied the dynamics of tearing modes in magnetic fusion experiments under the influence of resonant error-fields and/or eddy currents excited in the vacuum vessel. The interested reader is referred to Refs. 33–44, in addition to those papers which have already been mentioned. The present study differs from previous studies in three respects. First, the analysis is carried out using RFP, rather than tokamak, orderings. Note that the tokamak ordering is simply a subset of the RFP ordering, obtained by taking the limit $m^2 \gg n^2 \epsilon^2$. Hence, in this respect, the present study is *more general* than most previous studies. Secondly, this paper does not assume the existence of a fixed-width region of the plasma, centered on the rational surface, i.e., a *magnetic island*, which corotates with the mode. Instead, a far more physical model is adopted in which the width of the plasma region which corotates with the mode is determined by plasma *viscosity*, and, therefore, *varies* as the mode angular acceleration varies. Finally, this paper deals with error-field and vacuum vessel eddy current effects *simultaneously*, and presents, for the first time, a *comprehensive theory* of the influence of a resistive vacuum vessel on the error-field locking and unlocking thresholds.

III. DERIVATION OF PHASE EVOLUTION EQUATIONS

A. Introduction

The standard approach to tearing mode dynamics in magnetic fusion experiments, as exemplified by the classic paper of Zohm *et al.*,[40] leads to the following set of phase evolution equations:

$$\frac{d\phi}{d\hat{t}} = v, \tag{42}$$

$$\hat{I}_\phi \frac{dv}{d\hat{t}} + (v-1) + \frac{a_s^2}{4} \frac{v}{v_s^2 + v^2} + \frac{a_s a_c}{\sqrt{v_l}} \sin \phi = 0. \tag{43}$$

Here, $\phi \equiv \varphi_s - \varphi_c$ is the helical phase of the tearing mode measured with respect to that of the error-field, $v \equiv \hat{\Omega}_s$ is the normalized toroidal angular velocity of the mode, and $\hat{I}_\phi = I_\phi n \Omega_s^{(0)} \tau_V / [4\pi^2 r_s^2 R_0^3 \rho(r_s)]$ is the normalized toroidal moment of inertia of the fixed region of the plasma which is assumed to corotate with the mode (I_ϕ is the actual moment of inertia of this region). The first term in Eq. (43) represents the inertia of the corotating region, the second term is the restoring torque due to viscous coupling with the remainder of the plasma, the third term represents the braking torque due to eddy currents excited in the resistive shell, and the fourth term is the locking torque due to the resonant error-field. Although the above set of equations does not, in gen-

eral, possess an analytic solution, its numerical solution is very straightforward. Hence, this set of equations (or some closely related variant) is used extensively by experimentalists to interpret mode locking data obtained from magnetic fusion experiments.[45–47]

Instead of assuming the existence of a fixed-width region of the plasma which corotates with the mode, Eqs. (37)–(41) take into account the fact that the width of the corotating region is actually determined by the viscous coupling of the plasma in the immediate vicinity of the rational surface to the bulk plasma, and is, therefore, *variable*. Unfortunately, Eqs. (37)–(41) are far more complicated than Eqs. (42)–(43), since the former set of equations contains a *partial differential equation*, whereas the latter set merely consists of two coupled, first-order, *ordinary differential equations*. Certainly, in their present form, the improved phase evolution equations, Eqs. (37)–(41), are too complicated for convenient use by experimentalists. The aim of the remainder of this section is to reduce this set of equations to a more manageable form via the judicious use of approximations.

B. Derivation

According to Eq. (38), the electromagnetic torque acting in the vicinity of the rational surface consists of two parts: the *steady* torque due to eddy currents excited in the resistive shell, and the *oscillating* torque due to the resonant error-field. It is, therefore, natural to suppose that the (normalized) perturbed rotation profile of the plasma, $\Delta\hat{\Omega}(\hat{r},\hat{t})$, consists of a steady component, $V_0(\hat{r})$, driven by the eddy current torque, and an oscillating component, $V_1(\hat{r},\hat{t})$, driven by the error-field torque. In other words,

$$\Delta\hat{\Omega}(\hat{r},\hat{t}) = V_0(\hat{r}) + V_1(\hat{r},\hat{t}). \qquad (44)$$

Suppose that the steady component of $\Delta\hat{\Omega}(\hat{r},\hat{t})$ is simply taken to be the perturbed rotation profile calculated in the *absence* of the error-field. It follows that[19,24]

$$V_0(\hat{r}) = (v_0 - 1)$$
$$\times \begin{cases} 1 & \text{for } \hat{r} \leqslant 1 \\ \int_{\hat{r}}^{\hat{a}} d\hat{r}/\hat{r}\hat{\mu} \Big/ \int_1^{\hat{a}} d\hat{r}/\hat{r}\hat{\mu} & \text{for } 1 < \hat{r} \leqslant \hat{a} \end{cases}$$
$$\qquad (45)$$

where

$$1 - v_0 = \frac{a_s^2}{4} \frac{v_0}{v_s^2 + v_0^2}. \qquad (46)$$

Here, v_0 is the steady (normalized) angular velocity of the mode in the presence of the resistive shell, but the absence of the error-field. It is generally convenient to search for the physical roots of the above expression by converting it into a dynamical equation,

$$\frac{d^2 v_0}{d\hat{t}^2} + \lambda \frac{dv_0}{d\hat{t}} = 1 - v_0 - \frac{a_s^2}{4}\frac{v_0}{v_s^2 + v_0^2}. \qquad (47)$$

Here, λ is a positive constant chosen so as to optimize the convergence of the solution of the above equation towards a final fixed-point [which is equivalent to the physical root of Eq. (46)].

Equations (44), (45), and (46) can be combined with the original phase evolution equations (37)–(41) to give a new set of phase evolution equations,

$$\frac{\hat{r}\hat{\rho}}{4J^2 v_l}\frac{\partial V_1}{\partial \hat{t}} - \frac{\partial}{\partial \hat{r}}\left(\hat{r}\hat{\mu}\frac{\partial V_1}{\partial \hat{r}}\right) = -\frac{\hat{T}_1}{J}\delta(\hat{r}-1), \qquad (48)$$

$$\hat{T}_1 = \frac{a_s^2}{4}\left\{\frac{v}{v_s^2+v^2} - \frac{v_0}{v_s^2+v_0^2}\right\} + \frac{a_s a_c}{\sqrt{v_l}}\sin\phi, \qquad (49)$$

$$\frac{\partial V_1(0,\hat{t})}{\partial \hat{r}} = 0, \qquad (50)$$

$$V_1(\hat{a},\hat{t}) = 0, \qquad (51)$$

$$v - v_0 = V_1(1,\hat{t}). \qquad (52)$$

Here, $v \equiv d\phi/d\hat{t}$ is the (normalized) angular velocity of the mode in the presence of both the resistive shell and the error-field.

According to Eq. (49), the electromagnetic torque driving the oscillating component of the perturbed plasma rotation profile consists of two parts; the time-varying component of the eddy current braking torque induced by error-field driven oscillations of the mode angular velocity v about its steady value v_0, and the oscillating torque due to the error-field. The latter torque modulates like $\sin\phi$, where ϕ is the helical phase of the mode measured with respect to that of the error-field. It is the fundamental assumption of this derivation that the former torque also modulates like $\sin\phi$. This assumption can be justified *a posteriori*; it is found to hold exactly for locked modes, to be a fairly good approximation for most rotating modes, and to only seriously break down in a narrow region of parameter space close to the error-field locking threshold. Hence, this assumption—which greatly simplifies the analysis—can be used, with a fair degree of confidence, to map out the nature of the various time asymptotic solutions of the above set of phase evolution equations in parameter space.

The fundamental assumption is equivalent to the adoption of the following trial solution to Eqs. (48)–(52):

$$V_1(\hat{r},\hat{t}) = -i\bar{V}_1(\hat{r})\exp(i\phi). \qquad (53)$$

Obviously, the actual solution is the *real part* of the above expression. Equations (48), (50), (51), and (53) possess simple analytic solutions in two limits. The first limit corresponds to $v \ll v_l$, in which case

$$\bar{V}_1(\hat{r}) \simeq V_s \begin{cases} 1 & \text{for } \hat{r} \leqslant 1 \\ \int_{\hat{r}}^{\hat{a}} d\hat{r}/\hat{r}\hat{\mu} \Big/ \int_1^{\hat{a}} d\hat{r}/\hat{r}\hat{\mu} & \text{for } 1 < \hat{r} \leqslant \hat{a} \end{cases}$$
$$\qquad (54)$$

The second limit corresponds to $v \gg v_l$, in which case

3616   Phys. Plasmas, Vol. 7, No. 9, September 2000

R. Fitzpatrick and E. P. Yu

$$\bar{V}_1(\hat{r}) \simeq V_s \begin{cases} \exp[+\sqrt{iv/v_l}(\hat{r}-1)/(2J)] & \text{for } \hat{r} \leq 1 \\ \exp[-\sqrt{iv/v_l}(\hat{r}-1)/(2J)] & \text{for } 1 < \hat{r} \leq \hat{a} \end{cases}$$

$$(55)$$

The above expressions indicate that when the mode rotation velocity v lies well below the critical value v_l then the oscillating component of the perturbed angular velocity profile, driven by the error-field, extends over the whole plasma. On the other hand, when the rotation velocity greatly exceeds v_l then the oscillating component of the perturbed velocity profile becomes *localized* in the vicinity of the rational surface. In this paper, it is assumed that if a magnetic island structure exists at the rational surface then its radial width is always much less than the radial width of the oscillating velocity profile. Hence, it is always *viscosity* which determines the extent of the region of the plasma which corotates with the mode, rather than the magnetic island width. For the typical island widths, mode rotation velocities, and momentum confinement time scales encountered in present-day magnetic fusion experiments, this assumption is perfectly reasonable.

Now, according to Eqs. (54) and (55),

$$\bar{T}_1 = J\left[\hat{r}\hat{\mu}\frac{d\bar{V}_1}{d\hat{r}}\right]_{1-}^{1+} = -V_s \begin{cases} \sqrt{iv/v_l} & \text{for } v \gg v_l \\ 1 & \text{for } v \ll v_l \end{cases} \quad (56)$$

It is a reasonably good approximation to write

$$\bar{T}_1 = -V_s R, \qquad (57)$$

where

$$R \simeq \sqrt{1 + iv/v_l}. \qquad (58)$$

In the Appendix, the above approximation is discussed and justified.

Let $V_s = |V_s| \exp(i\theta_s)$ and $R = |R| \exp(i\theta_R)$. According to Eqs. (52)–(57),

$$v - v_0 = V_1(1,\hat{t}) = |V_s| \sin(\phi + \theta_s), \qquad (59)$$

$$\hat{T}_1(\hat{t}) = -|V_s||R| \sin(\phi + \theta_s + \theta_R). \qquad (60)$$

Now, it follows from the fundamental assumption (53) that

$$\frac{dV_1(1,\hat{t})}{d\hat{t}} = iv V_1(1,\hat{t}), \qquad (61)$$

which yields

$$\frac{dv}{d\hat{t}} = \frac{dV_1(1,\hat{t})}{d\hat{t}} = v|V_s|\cos(\phi + \theta_s). \qquad (62)$$

It is clear that the fundamental assumption boils down to the assertion that the time variation of the mode angular velocity v is dominated by the modulation of the helical phase ϕ, rather than any variation in the amplitude $|V_s|$ or the phase angle θ_s.

Equations (59), (60), and (62) yield

$$\hat{T}_1(\hat{t}) = -|V_s||R|\cos(\phi + \theta_s)\sin\theta_R - |V_s||R|\sin(\phi + \theta_s)\cos\theta_R,$$

$$= -|R|\sin\theta_R \frac{1}{v}\frac{dv}{d\hat{t}} - |R|\cos\theta_R(v - v_0),$$

$$\simeq -\frac{\{[1+(v/v_l)^2]^{1/2}-1\}^{1/2}}{\sqrt{2}|v|}\frac{dv}{d\hat{t}}$$

$$-\frac{\{[1+(v/v_l)^2]^{1/2}+1\}^{1/2}}{\sqrt{2}}(v - v_0), \qquad (63)$$

where use has been made of Eq. (58). Finally, the above equation can be combined with Eqs. (46) and (49) to give

$$\frac{\{[1+(v/v_l)^2]^{1/2}-1\}^{1/2}}{\sqrt{2}|v|}\frac{dv}{d\hat{t}}$$

$$+\frac{\{[1+(v/v_l)^2]^{1/2}+1\}^{1/2}}{\sqrt{2}}(v - v_0) + (v_0 - 1)$$

$$+\frac{a_s^2}{4}\frac{v}{v_s^2 + v^2} + \frac{a_s a_c}{\sqrt{v_l}}\sin\phi = 0. \qquad (64)$$

C. Discussion

According to the previous analysis, the improved phase evolution equations (37)–(41) can be reduced to the following set of four, coupled, first-order, ordinary differential equations:

$$\frac{d\phi}{d\hat{t}} = v, \qquad (65)$$

$$\frac{\{[1+(v/v_l)^2]^{1/2}-1\}^{1/2}}{\sqrt{2}|v|}\frac{dv}{d\hat{t}}$$

$$+\frac{\{[1+(v/v_l)^2]^{1/2}+1\}^{1/2}}{\sqrt{2}}(v - v_0) + (v_0 - 1)$$

$$+\frac{a_s^2}{4}\frac{v}{v_s^2 + v^2} + \frac{a_s a_c}{\sqrt{v_l}}\sin\phi = 0, \qquad (66)$$

$$\frac{dv_0}{d\hat{t}} = a_0, \qquad (67)$$

$$\frac{da_0}{d\hat{t}} + \lambda a_0 + (v_0 - 1) + \frac{a_s^2}{4}\frac{v_0}{v_s^2 + v_0^2} = 0. \qquad (68)$$

The physical dynamical variables are ϕ—the helical phase of the mode measured with respect to that of the error-field—and v—the normalized angular velocity of the mode. Recall that Eqs. (67) and (68) are merely a numerical device for finding the appropriate roots of Eq. (46), and have no direct physical interpretation. However, the dynamical variable v_0 is interpreted as the steady component of v obtained by balancing plasma viscosity against the eddy current braking torque, whilst neglecting the oscillating error-field torque. The parameter a_s [defined in Eq. (32)] is the normalized mode amplitude, a_c [defined in Eq. (33)] is the normalized amplitude of the error-field, v_s [defined in Eq. (34)] is the critical value of v above which the resistive shell starts to act like a perfect conductor, and v_l [defined in Eq. (35)] is the critical value of v above which the oscillating component of the perturbed plasma rotation profile, driven by the error-field, becomes localized in the vicinity of the rational sur-

face. In addition, λ is an optional, $O(1)$, positive parameter, with no direct physical significance, which is used to facilitate the numerical solution of the above equations.

Virtually all of the physics content of the above set of phase evolution equations resides in Eq. (66), which is interpreted as the angular equation of motion of the mode. The first term represents the inertia of the region of the plasma which corotates with the mode, the second term is the restoring torque due to viscous coupling between the plasma in the immediate vicinity of the rational surface and the oscillating component of the perturbed plasma rotation profile, the third term represents the restoring torque due to viscous coupling between the plasma in the immediate vicinity of the rational surface and the steady component of the perturbed plasma rotation profile, the fourth term is the braking torque due to eddy currents excited in the resistive shell, and the fifth term represents the locking torque due to the error-field.

In the limit $v_l \gg 1$, Eqs. (65) and (66) reduce to

$$\frac{d\phi}{d\hat{t}} = v, \tag{69}$$

$$\frac{1}{2v_l} \frac{dv}{d\hat{t}} + (v-1) + \frac{a_s^2}{4} \frac{v}{v_s^2 + v^2} + \frac{a_s a_c}{\sqrt{v_l}} \sin\phi = 0. \tag{70}$$

Note that since the variable v_0 does not appear in these equations, they form a complete set, and Eqs. (67) and (68) are redundant. Of course, the above pair of phase evolution equations has the same form as the Zohm equations, (42) and (43). However, for the typical momentum confinement time scales and mode rotation velocities observed in present-day RFPs, the parameter v_l is usually much less than unity. [The approximate formula for this parameter is $v_l \sim \chi_\perp / \Omega_s^{(0)} a^2$, where $\chi_\perp$ is the anomolous momentum diffusivity, $\Omega_s^{(0)}$ is the typical dynamo mode rotation frequency, and a is the plasma minor radius. The anomolous momentum diffusion in the core of present-day RFPs is predominately due to magnetic fluctuations: the typical diffusivity is $\chi_\perp \sim 50 \, \mathrm{m/s}^2$.[25] Likewise, the typical mode rotation frequency is $\Omega_s^{(0)} \sim 5 \times 10^3 \, \mathrm{rad/s}$, and the typical minor radius is $a \sim 0.5 \, \mathrm{m}$.[16] Hence, $v_l \sim 0.04$ in present-day RFPs. This estimate is sufficiently small compared to unity that we can be certain that all present-day RFPs lie in the parameter regime $v_l \ll 1$, as assumed in this paper. Another important assumption, made in this paper, is that the radial width of the oscillating component of the perturbed velocity profile is much wider that the radial magnetic island width, W, at the rational surface. This assumption is valid provided $W/r_s < \sqrt{v_l} \sim 0.2$, which is reasonably well satisfied in present-day RFPs.] In this parameter regime, the Zohm equations are replaced by Eqs. (65)–(68). Fortunately, the numerical solution of this new set of phase evolution equations is almost as straightforward as that of the Zohm equations. Equations (65)–(68) are more complicated than the Zohm equations because they contain additional physics; namely, a self-consistent calculation of the radial extent of the region of the plasma which corotates with the mode; the width of this region being determined by plasma viscosity.

IV. ANALYSIS OF PHASE EVOLUTION EQUATIONS

A. Resistive shell braking and release thresholds

Suppose that the amplitude of the resonant error-field approaches zero (i.e., $a_c \to 0$). In this limit, the phase evolution equations (65)–(68) simplify greatly to give $v = v_0$, $dv/d\hat{t} = a_0 = 0$, and

$$1 - v = \frac{a_s^2}{4} \frac{v}{v_s^2 + v^2}. \tag{71}$$

Note that in the absence of the error-field the mode rotates with a *steady* velocity. The solution of the above equation in the physically relevant regime $v_s \ll 1$ is fairly straightforward. There are two branches of solutions. First, there is a *rapidly rotating* branch,

$$v \simeq \tfrac{1}{2} + \tfrac{1}{2}\sqrt{1 - a_s^2}, \tag{72}$$

on which the mode rotation velocity is sufficiently high that the resistive shell acts like a perfect conductor. Secondly, there is a *slowly rotating* branch,

$$v \simeq \frac{a_s^2}{8} \{ 1 - \sqrt{1 - (\sqrt{8v_s}/a_s)^4} \}, \tag{73}$$

on which the mode rotation velocity is sufficiently low that the mode eigenfunction can penetrate through the resistive shell. Moreover, there is a *forbidden band* of (normalized) mode rotation velocities,

$$v_s < v < 1/2, \tag{74}$$

separating these two branches. When the normalized mode amplitude a_s exceeds the *resistive shell braking threshold*,

$$(a_s)_b = 1, \tag{75}$$

then the rapidly rotating branch of solutions ceases to exist, and the mode makes a transition from the rapidly to the slowly rotating branch (assuming that it starts off on the former branch). When the normalized mode amplitude falls below the *resistive shell release threshold*,

$$(a_s)_r = \sqrt{8v_s}, \tag{76}$$

then the slowly rotating branch of solutions ceases to exist, and the mode makes a transition from the slowly to the rapidly rotating branch (assuming that it starts off on the former branch). There is considerable *hysteresis* in the resistive shell braking/release cycle, since the release threshold is generally significantly smaller than the braking threshold. Note that the inevitable penetration of the mode eigenfunction through the resistive shell on the slowly rotating branch of solutions has a destabilizing effect on the mode, leading to a somewhat larger saturated amplitude (i.e., larger a_s) on the slowly rotating branch, and, hence, to some deepening of this hysteresis.

Figure 1 shows an example hysteresis diagram for the resistive shell braking/release cycle, calculated for $v_s = 0.05$.
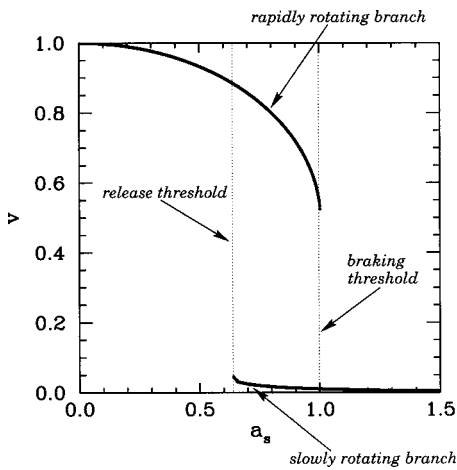
FIG. 1. The hysteresis diagram for the resistive shell braking/release cycle, calculated for $v_s = 0.05$. The normalized mode rotation velocity v is plotted as a function of the normalized mode amplitude a_s.

FIG. 2. The rotating branch of solutions, calculated for $a_c = 1$ and $v_l = 0.05$. The maximum and minimum values of the normalized mode rotation velocity v are plotted as functions of the normalized mode amplitude a_s.

Note that the above theoretical results were first derived in Ref. 24, and were later confirmed experimentally in Ref. 45.

B. Error-field locking and unlocking thresholds

Suppose that the parameter v_s goes to infinity. In this limit, the resistive shell acts like a perfect conductor, and there is zero eddy current braking torque. Furthermore, the phase evolution equations (65)–(68) simplify greatly to give $v_0 = 1$, $a_0 = 0$, and

$$\frac{d\phi}{d\hat{t}} = v, \tag{77}$$

$$\frac{\{[1+(v/v_l)^2]^{1/2}-1\}^{1/2}}{\sqrt{2}|v|} \frac{dv}{d\hat{t}}$$

$$+ \frac{\{[1+(v/v_l)^2]^{1/2}+1\}^{1/2}}{\sqrt{2}}(v-1) + \frac{a_s a_c}{\sqrt{v_l}}\sin\phi = 0. \tag{78}$$

The numerical solution of the above pair of equations in the physically relevant regime $v_l \ll 1$ is fairly straightforward. There are two branches of solutions. First, there is a *rotating branch* on which the mode angular velocity v is modulated periodically, as the mode rotates, by the oscillating error-field torque. Secondly, there is a *locked branch* on which the mode is held stationary (i.e., $v=0$) via the balance of the error-field and viscous restoring torques. For the locked branch, the above phase evolution equations simplify further to give

$$\frac{a_s a_c}{\sqrt{v_l}}\sin\phi = 1. \tag{79}$$

Figure 2 illustrates the nature of the rotating branch of solutions. It can be seen that as the normalized mode amplitude a_s increases the amplitude of the error-field driven oscillations in the normalized mode rotation velocity v also
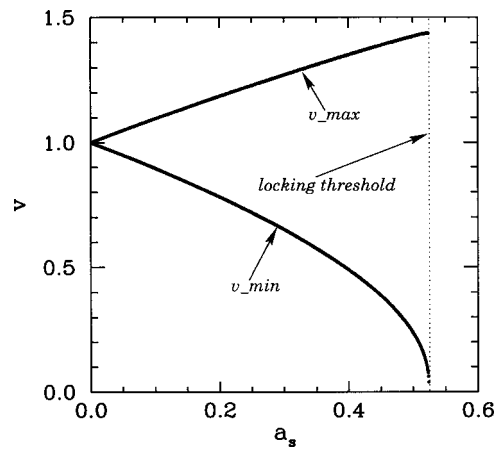
increases. When the product of the normalized mode amplitude a_s and the normalized error-field amplitude a_c exceeds the *error-field locking threshold*,

$$(a_s a_c)_l \simeq 0.51, \tag{80}$$

then the rotating branch of solutions ceases to exist, and the mode makes a transition from the rotating to the locked branch (assuming that it starts off on the former branch). Note that the error-field locking threshold (which is determined numerically) is a very weak function of v_l. Note, further, that the disappearance of the rotating branch of solutions corresponds to the point at which the minimum velocity of the mode is reduced to zero by the error-field.

Figure 3 illustrates the nature of the locked branch of solutions. It can be seen that as the normalized mode amplitude a_s decreases the locking angle ϕ increases. According to Eq. (79), when the product of the normalized mode amplitude a_s and the normalized error-field amplitude a_c falls below the *error-field unlocking threshold*,
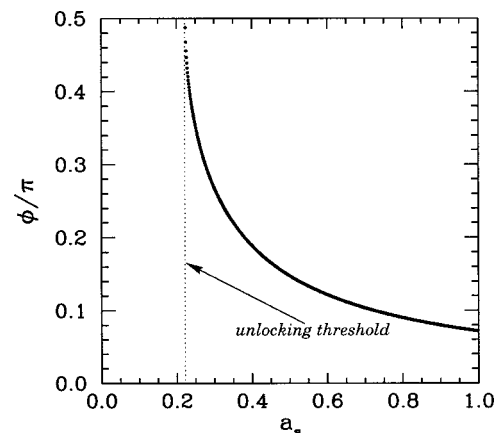
$$(a_s a_c)_u = \sqrt{v_l}, \tag{81}$$

FIG. 3. The locked branch of solutions, calculated for $a_c = 1$ and $v_l = 0.05$. The locking angle ϕ is plotted as a function of the normalized mode amplitude a_s.
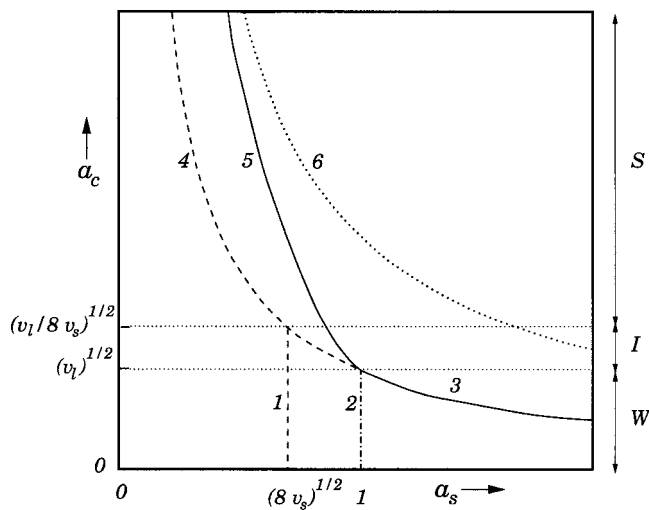
FIG. 4. A schematic diagram showing the various threshold curves associated with the phase evolution of a dynamo mode in a RFP in the presence of both a resistive shell and a resonant error-field. The curves are plotted in normalized mode amplitude a_s vs normalized error-field amplitude a_c space. Curve 1 is the resistive shell release threshold; curve 2 is the resistive shell braking threshold; curve 3 is the combined error-field locking and unlocking threshold; curve 4 is the error-field unlocking threshold; curve 5 is the error-field locking threshold; and curve 6 is the error-field locking threshold in the absence of the resistive shell. The extents of the strong (S), intermediate (I), and weak (W) error-field regimes are also indicated.

then the locked branch of solutions ceases to exist, and the mode makes a transition from the locked to the rotating branch (assuming that it starts off on the former branch). Note that the disappearance of the locked branch of solutions corresponds to the point at which the locking angle ϕ reaches $\pi/2$.

There is considerable *hysteresis* in the error-field locking/unlocking cycle, since the unlocking threshold is generally significantly smaller than the locking threshold. The origin of this hysteresis is the strong variation in the radial width of the plasma region which corotates with the mode as the normalized mode velocity v changes. Of course, the more efficient interaction between the mode and the error-field on the locked branch of solutions has a destabilizing effect on the mode, leading to a somewhat larger saturated amplitude (i.e., larger a_s) on the locked branch, and, hence, to some deepening of this hysteresis.

C. Resistive shell modified error-field locking and unlocking thresholds

The simultaneous presence of a resistive shell and a static error-field necessitates the use of the full set of phase evolution equations (65)–(68). Fortunately, the numerical solution of these equations is a relatively straightforward task. A comprehensive parameter scan, in the physically relevant regime v_l, $v_s \ll 1$, leads to the diagram shown in Fig. 4. This diagram indicates the *approximate* locations of all the various threshold curves in normalized mode amplitude a_s vs normalized error-field amplitude a_c space. Note that the locations of these curves are determined numerically. The curve labeled 1 represents the resistive shell release threshold: the approximate formula for this curve is $a_s = \sqrt{8v_s}$ for

$a_c \lesssim \sqrt{v_l/8v_s}$. The curve labeled 2 represents the resistive shell braking threshold: the approximate formula for this curve is $a_s = 1$ for $a_c \lesssim \sqrt{v_l}$. The curve labeled 3 represents the combined error-field locking and unlocking threshold; the approximate formula for this curve is $a_s a_c = \sqrt{v_l}$ for $a_s \gtrsim 1$. The curve labeled 4 represents the error-field unlocking threshold: the approximate formula for this curve is $a_s a_c = \sqrt{v_l}$ for $a_s < 1$. The curve labeled 5 represents the error-field locking threshold; the approximate formula for this curve is $a_s a_c = [\sqrt{v_l}a_s^2 + 0.51(1 - a_s^2)]$ for $a_s < 1$. Finally, the curve labeled 6 represents the error-field locking threshold in the absence of the resistive shell; the approximate formula for this curve is $a_s a_c = 0.51$.

Note that the location of the error-field unlocking threshold curve (curves 3 and 4 in Fig. 4) is *unaffected* by the presence of the resistive shell. This is as expected, since a resistive shell exerts zero torque on a locked mode, and, therefore, cannot affect its unlocking threshold. On the other hand, the location of the error-field locking threshold curve in the presence of the resistive shell (curves 3 and 5 in Fig. 4) is different from that in the absence of the shell (curve 6 in Fig. 4). In fact, it can be seen that the critical value of the product $a_s a_c$ above which a transition to a locked mode is triggered is always *reduced* in the presence of the resistive shell. In other words, the resistive shell acts as a *catalyst* for the formation of an error-field locked mode. Incidentally, the use of the term "catalyst" here is appropriate, since the resistive shell plays no role in the dynamics of the mode once it has locked to the error-field.

Figure 4 suggests the existence of *three* broad regimes of behavior, depending on the value of the normalized error-field amplitude a_c. The *weak error-field regime* corresponds to

$$a_c < \sqrt{v_l}. \tag{82}$$

The *intermediate error-field regime* corresponds to

$$\sqrt{v_l} \lesssim a_c \lesssim \sqrt{v_l/8v_s}. \tag{83}$$

Finally, the *strong error-field regime* corresponds to

$$a_c > \sqrt{v_l/8v_s}. \tag{84}$$

These three regimes are described in the following.

D. The weak error-field regime

Figure 5 illustrates the typical behavior encountered in the weak error-field regime. As the normalized mode amplitude a_s is gradually increased from a small value, the time-asymptotic solution starts off on the rapidly rotating branch of solutions, and then makes a transition to the slowly rotating branch when the resistive shell braking threshold (curve 2 in Fig. 4) is reached. The solution makes a second transition to the locked branch when the error-field locking threshold (curve 3 in Fig. 4) is reached. As a_s is gradually decreased from a large value, the solution starts off on the locked branch of solutions, and then makes a transition to the slowly rotating branch when the error-field unlocking threshold (curve 3 in Fig. 4) is reached. The solution makes a
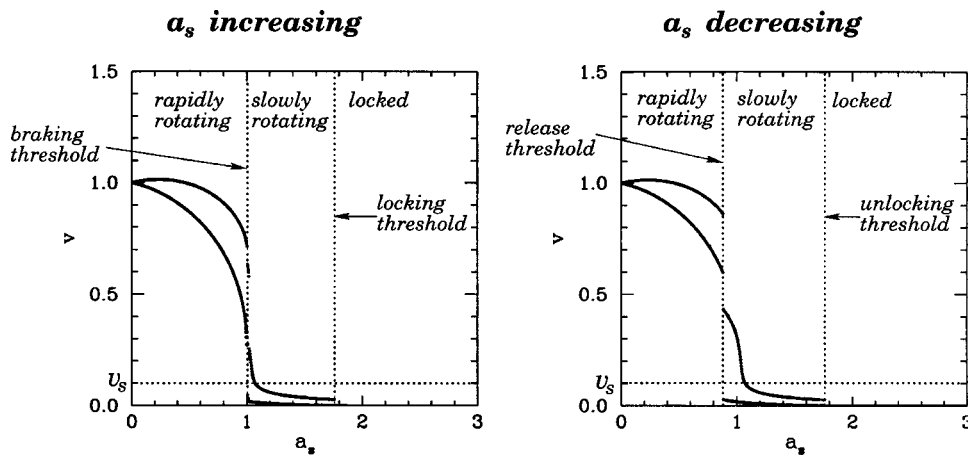
FIG. 5. The weak error-field regime. The maximum and minimum values of the normalized rotation velocity v are plotted as functions of the normalized mode amplitude a_s for $a_c = 0.12$, $v_s = 0.1$, and $v_l = 0.05$. The cases where the normalized mode amplitude a_s is increasing and decreasing are shown separately.

second transition to the rapidly rotating branch when the resistive shell release threshold (curve 1 in Fig. 4) is reached.

Note that in the weak error-field regime there is hysteresis in the resistive shell braking/release cycle but there is *no hysteresis* in the error-field locking/unlocking cycle.

In order to help explain the somewhat surprising absence of hysteresis in the error-field locking/unlocking cycle, Fig. 6 shows a typical slowly rotating solution which lies close to the error-field locking threshold in parameter space. It can be seen that the mode rotates *intermittently*. In other words, the mode remains locked for a certain period of time, then suddenly executes a single rotation, remains locked for the same period of time, then suddenly executes another rotation, and so on. As the error-field locking threshold is approached in parameter space, the time interval between these intermittent rotation events increases rapidly, and effectively becomes infinite as the threshold is attained. Hence, there is a completely *reversible* (i.e., hysteresis free) transition between a slowly rotating mode and a locked mode as the error-field locking/unlocking threshold is crossed. This reversible transition should be contrasted with the irreversible transition illustrated in Fig. 8 below. The latter transition is typical of the behavior of the error-field locking/unlocking cycle in the absence of a resistive shell.

It is important to note that the resistive shell is unable to remove those components of the hysteresis in the error-field locking/unlocking cycle which are associated with the destabilization of the mode when its eigenfunction is able to penetrate through the shell, or with the destabilization of the mode due to the more efficient interaction with the error-field when it is non-rotating.

It is clear that in the weak error-field regime the catalysis of locked mode formation by the resistive shell operates so effectively that a locked mode forms as soon as a locked mode solution becomes a possibility (i.e., as soon as the error-field unlocking threshold is exceeded).

E. The intermediate error-field regime

Figure 7 illustrates the typical behavior encountered in the intermediate error-field regime. As the normalized mode amplitude a_s is gradually increased from a small value, the time-asymptotic solution starts off on the rapidly rotating branch of solutions, and then makes a direct transition to the locked branch when the error-field locking threshold (curve 5 in Fig. 4) is reached. As a_s is gradually decreased from a large value, the solution starts off on the locked branch of solutions, and then makes a transition to the slowly rotating branch when the error-field unlocking threshold (curve 4 in Fig. 4) is reached. The solution makes a second transition to the rapidly rotating branch when the resistive shell release threshold (curve 1 in Fig. 4) is reached.

Note that in the intermediate error-field regime the slowly rotating branch of solutions is only accessible when the normalized mode amplitude a_s is decreasing. Note, also,
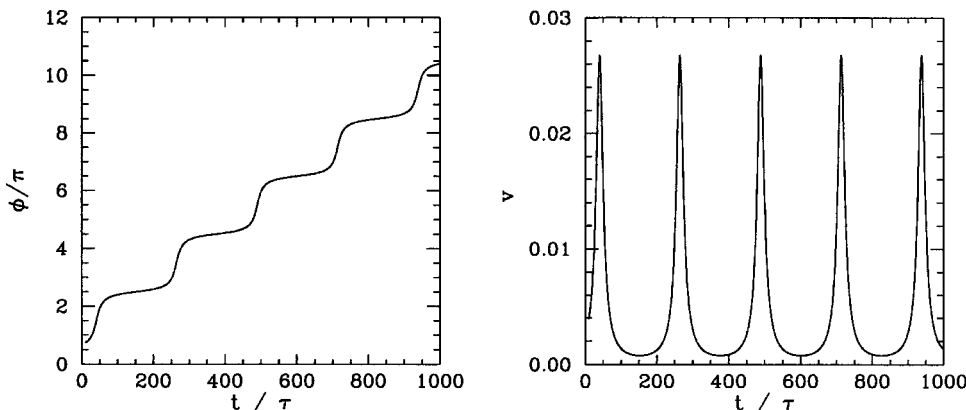

FIG. 6. A slowly rotating solution which lies close to the error-field locking threshold. The angular position ϕ and the normalized rotation velocity v of the mode are plotted as functions of t/τ, where τ is the unperturbed mode rotation period, for $a_s = 1.75$, $a_c = 0.12$, $v_s = 0.1$, and $v_l = 0.05$.
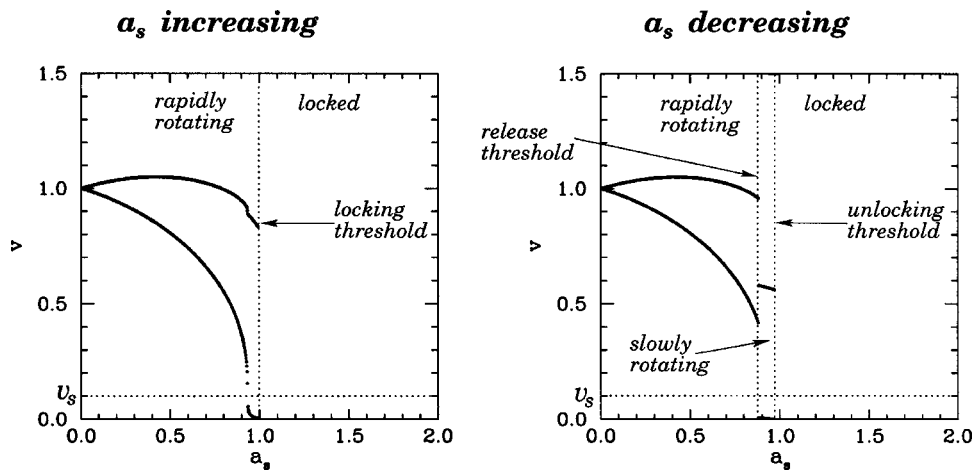
a_s increasing

a_s decreasing

FIG. 7. The intermediate error-field regime. The maximum and minimum values of the normalized rotation velocity v are plotted as functions of the normalized mode amplitude a_s for $a_c = 0.23$, $v_s = 0.1$, and $v_l = 0.05$. The cases where the normalized mode amplitude a_s is increasing and decreasing are shown separately.

that there is now a small amount of hysteresis in the error-field locking/unlocking cycle.

F. The strong error-field regime

Figure 8 illustrates the typical behavior encountered in the strong error-field regime. As the normalized mode amplitude a_s is gradually increased from a small value, the time-asymptotic solution starts off on the rapidly rotating branch of solutions, and then makes a direct transition to the locked branch when the error-field locking threshold (curve 5 in Fig. 4) is reached. As a_s is gradually decreased from a large value, the solution starts off on the locked branch of solutions, and then makes a direct transition to the rapidly rotating branch when the error-field unlocking threshold (curve 4 in Fig. 4) is reached.

Note that in the strong error-field regime the slowly rotating branch of solutions no longer exists. Note, also, that there is strong hysteresis in the error-field locking/unlocking cycle in this regime. In fact, as the normalized error-field amplitude a_c increases beyond the critical value $\sqrt{v_l/8v_s}$, the resistive shell has progressively less effect on the location of the error-field locking threshold, which quickly reverts to that calculated in the absence of a shell.

V. APPLICATION TO EXPERIMENTS

Consider the typical RFX plasma equilibrium investigated in Ref. 19. The parameters for this equilibrium are $I_\phi = 600 \, \text{kA}$, $\epsilon_a = 0.23$, $F \equiv B_\phi(a)/\langle B_\phi \rangle = -0.2$, and $\Theta \equiv B_\theta(a)/\langle B_\phi \rangle = 1.56$. The characteristic dynamo mode for this equilibrium is the $m = 1$, $n = 9$ mode. Making the same assumptions as those made in Sec. V B of Ref. 19, except that the plasma viscosity profile is now assumed to be radially *uniform* (for the sake of simplicity), the following estimated values for the parameters controlling the phase evolution of the 1,9 mode in RFX are obtained:

$$v_s \simeq 0.12, \tag{85}$$

$$v_l \simeq 0.013, \tag{86}$$

$$a_s \simeq 3.7, \tag{87}$$

$$a_c \simeq 380 \left(\frac{b_r^{1,9}}{|B|} \right)_c. \tag{88}$$

Here, it is assumed that the nominal island width of the 1,9 mode is 20% of the plasma minor radius. Furthermore, $(b_r^{1,9}/|B|)_c$ represents the ratio of the radial component of the

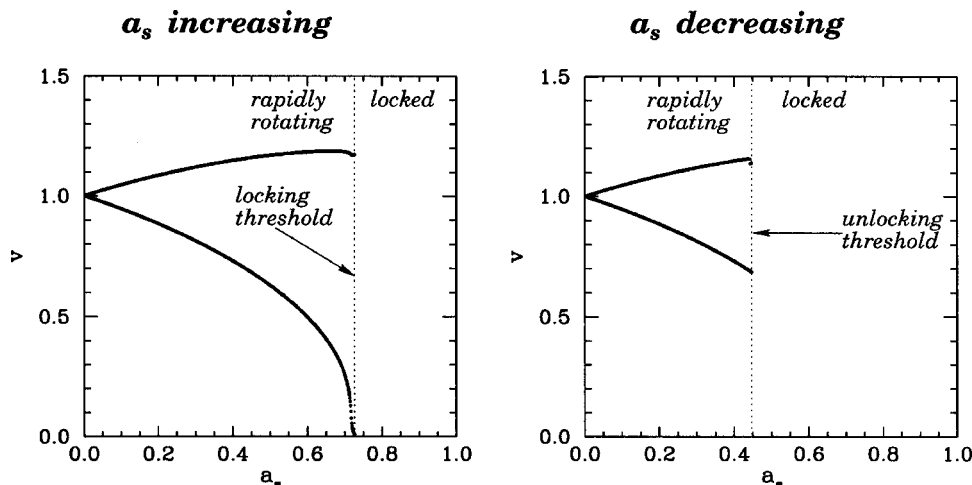## a_s increasing

a_s decreasing

FIG. 8. The strong error-field regime. The maximum and minimum values of the normalized rotation velocity v are plotted as functions of the normalized mode amplitude a_s for $a_c = 0.5$, $v_s = 0.1$, and $v_l = 0.05$. The cases where the normalized mode amplitude a_s is increasing and decreasing are shown separately.
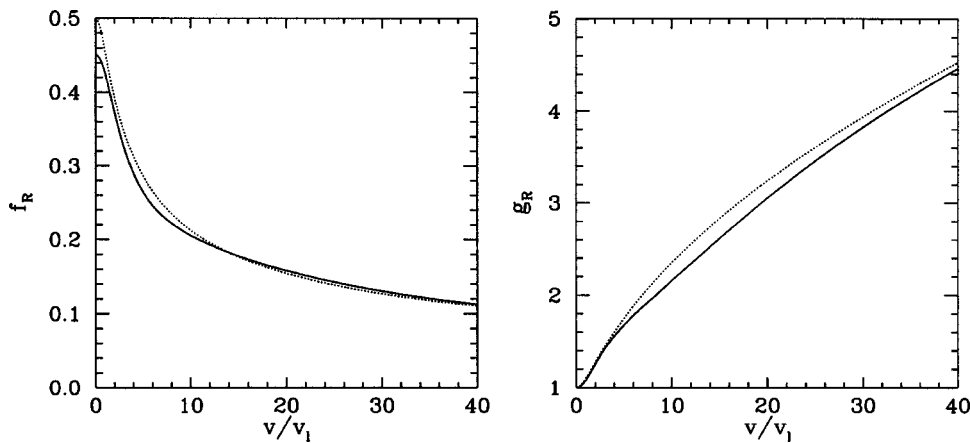
FIG. 9. The functions f_R and g_R, defined in Eq. (A3), plotted against the normalized mode phase velocity v/v_l. The solid lines show the exact forms for these functions, derived from Eq. (A2). The dotted lines show the approximate forms for the functions, derived from the approximation (A6). The calculations are performed for $\hat{a} = 1/0.7$.

1,9 harmonic of the error-field to the magnitude of the equilibrium magnetic field, evaluated at the radius of the conducting shell.

According to the analysis of Sec. IV, the locking and unlocking of the 1, 9 dynamo mode in RFX occurs in the *weak error-field regime*. Hence, the combined locking/unlocking threshold corresponds to the curve $a_s a_c = \sqrt{v_l}$ in parameter space. In the absence of the resistive shell, the unlocking threshold still corresponds to $a_s a_c = \sqrt{v_l}$, but the locking threshold becomes $a_s a_c = 0.51$. Hence, the critical error-field amplitude required to lock a typical dynamo mode in RFX is estimated to be

$$\left(\frac{b_r^{1,9}}{|B|} \right)_c \sim 8 \times 10^{-5}. \tag{89}$$

In the absence of the resistive vacuum vessel, the critical amplitude becomes

$$\left(\frac{b_r^{1,9}}{|B|} \right)_c \sim 4 \times 10^{-4}. \tag{90}$$

In other words, the resistive vacuum vessel in RFX reduces the critical error-field amplitude required to generate a locked mode by a factor of 5. This result suggests that the primary cause of the locked mode problems observed in RFX (and other large RFPs possessing thin resistive vacuum vessels, e.g., TPE-RX) is the high resistance vacuum vessel, which renders otherwise innocuous error-fields problematic.

VI. SUMMARY

This paper investigates the nonlinear dynamics of a typical dynamo mode in a RFP plasma in the presence of a resistive vacuum vessel and a resonant error-field. The achievements of this paper are as follows:

(1) The derivation of a fundamental set of phase evolution equations (37)–(41) (see Sec. II). These equations describe the phase evolution of a typical dynamo mode in a RFP under the influence of the braking torque due to eddy currents excited in a resistive vacuum vessel and the locking torque due to a resonant error-field. They are derived using the five physics-based assumptions listed and justified in Sec. II. Unfortunately, Eqs. (37)–(41)

are too complicated for convenient use by experimentalists whilst interpreting data or designing new RFP experiments.

(2) The reduction of the fundamental phase evolution equations to a more manageable set of four, coupled, first-order, ordinary differential equations (65)–(68) (see Sec. III). These equations represent an important extension of the well-known Zohm equations,[40] (42)–(43), which have been used extensively by experimentalists to interpret mode locking data obtained from magnetic fusion devices. The nature of the extension is the incorporation of a self-consistent calculation of the radial extent of the plasma region which corotates with the mode; the width of this region being determined by plasma viscosity.

(3) The numerical solution of Eqs. (65)–(68), so as to obtain a comprehensive theory of the influence of a resistive vacuum vessel on error-field locking and unlocking thresholds (see Sec. IV). This theory is encapsulated in Fig. 4, which shows the locations of all the various threshold curves for resistive shell braking, error-field locking, etc., in mode amplitude versus error-field amplitude space. Not surprisingly, a resistive vacuum vessel is found to have no effect on error-field unlocking thresholds. On the other hand, such a vessel is found to facilitate error-field locking; i.e., it reduces the error-field locking threshold. Under certain circumstances (i.e., in the weak error-field regime indicated in Fig. 4), this effect is so strong that a locked mode forms as soon as a locked solution becomes a possibility, i.e., as soon as the error-field unlocking threshold is exceeded. Note that, in the absence of a resistive vacuum vessel, the error-field unlocking threshold usually needs to be exceeded by a substantial factor before a locked mode forms.

(4) The application of the results obtained in Sec. IV to the problem of the locking of typical dynamo modes in RFX (see Sec. V). The thin resistive vacuum vessel in RFX is found to reduce the critical error-field amplitude required to generate a locked mode by a factor of 5. This result suggests that the high electrical resistance of the vacuum vessel is the primary cause of the locked mode problems in RFX, rather than the presence of excessively large error-fields.

In conclusion, this paper has developed a basic theoretical framework within which the phase evolution of rotating dynamo modes in RFPs can be analyzed. Hopefully, the physical insights and model equations obtained in this process will allow experimentalists to achieve a full understanding of why the so-called ''slinky mode'' locks in some reversed field pinch devices, but not in others. As explained in the Introduction, the locking of the slinky mode is currently an issue of outstanding importance in reversed field pinch research.

APPENDIX: AN EXACT FORM FOR THE PHASE EVOLUTION EQUATION

In the limit of a uniform density profile (i.e., $\hat{\rho}=1$) and a uniform viscosity profile (i.e., $\hat{\mu}=1$), Eqs. (48), (50), (51), and (53) can be solved exactly to give

$$
\bar{V}_1(\hat{r}) \simeq V_s \begin{cases} \dfrac{I_0(\sqrt{i\lambda}\hat{r})}{I_0(\sqrt{i\lambda})} & \text{for } \hat{r} \leq 1 \\[2ex] \dfrac{K_0(\sqrt{i\lambda}\hat{a})I_0(\sqrt{i\lambda}\hat{r}) - K_0(\sqrt{i\lambda}\hat{r})I_0(\sqrt{i\lambda}\hat{a})}{K_0(\sqrt{i\lambda}\hat{a})I_0(\sqrt{i\lambda}) - K_0(\sqrt{i\lambda})I_0(\sqrt{i\lambda}\hat{a})} & \text{for } 1 < \hat{r} \leq \hat{a} \end{cases},
$$

(A1)

where $J = \ln\hat{a}$ and $\lambda = (v/v_l)/(4J^2)$. Here, I_0 and K_0 are standard modified Bessel functions. In this limit, the function R, defined in Eqs. (56) and (57), takes the exact form

$$
R = J\sqrt{i\lambda}\left\{ \frac{I_1(\sqrt{i\lambda})}{I_0(\sqrt{i\lambda})} - \frac{K_0(\sqrt{i\lambda}\hat{a})I_1(\sqrt{i\lambda}) + K_1(\sqrt{i\lambda})I_0(\sqrt{i\lambda}\hat{a})}{K_0(\sqrt{i\lambda}\hat{a})I_0(\sqrt{i\lambda}) - K_0(\sqrt{i\lambda})I_0(\sqrt{i\lambda}\hat{a})} \right\}.
$$

(A2)

Repeating the analysis of Sec. III B, the above expression for R yields the following phase evolution equation for the mode:

$$
\frac{f_R}{v_l}\frac{dv}{d\hat{t}} + g_R(v - v_0) + (v_0 - 1) + \frac{a_s^2}{4}\frac{v}{v_s^2 + v^2} + \frac{a_s a_c}{\sqrt{v_l}}\sin\phi = 0,
$$

(A3)

where

$$
f_R = \frac{\text{Im}(R)}{(v/v_l)},
$$

(A4)

$$
g_R = \text{Re}(R).
$$

(A5)

The approximate expression

$$
R \simeq \sqrt{1 + iv/v_l},
$$

(A6)

employed in Sec. III B, leads to the following approximate forms for the functions f_R and g_R:

$$
f_{R\text{ approx}} = \frac{\{[1 + (v/v_l)^2]^{1/2} - 1\}^{1/2}}{\sqrt{2}|v/v_l|},
$$

(A7)

$$
g_{R\text{ approx}} = \frac{\{[1 + (v/v_l)^2]^{1/2} + 1\}^{1/2}}{\sqrt{2}}.
$$

(A8)

Figure 9 compares the above approximate forms for f_R and g_R with the exact forms derived from Eq. (A2). It can be seen that the agreement between the two sets of functions is excellent. This justifies the use of the approximate formula (A6) (which is far simpler than the exact formula) throughout the bulk of this paper.

[1]H. A. B. Bodin, Nucl. Fusion **30**, 1717 (1990).
[2]J. B. Taylor, Phys. Rev. Lett. **33**, 1139 (1974).
[3]B. Alper, M. K. Bevir, H. A. B. Bodin et al., Plasma Phys. Controlled Fusion **31**, 205 (1989).
[4]S. Ortolani, and D. D. Schnack, Magnetohydrodynamics of Plasma Relaxation (World Scientific, Singapore, 1993).
[5]F. Gnesotto, P. Sonato, W. R. Baker et al., Fusion Eng. Des. **25**, 335 (1995).
[6]Y. Yagi, S. Sekine, H. Sakakita et al., Fusion Eng. Des. **45**, 409 (1999).
[7]J. S. Sarff, N. E. Lanier, S. C. Prager, and M. R. Stoneking, Phys. Rev. Lett. **78**, 62 (1997).
[8]T. Tamano, W. D. Bard, C. Chu et al., Phys. Rev. Lett. **59**, 1444 (1987).
[9]A. Buffa, F. Gnesotto, V. Antoni, et al., in Controlled Fusion and Plasma Physics, in Proceedings of the 21st European Conference, Montpellier, 1994 (European Physical Society, Petit-Lancy, 1994), Vol. I, p. 458.
[10]R. Fitzpatrick, Phys. Plasmas **6**, 1168 (1999).
[11]T. Bolzonella, S. Ortolani, and J. S. Sarff, in Controlled Fusion and Plasma Physics, in Proceedings of the 25th European Conference, Prague, 1998 (European Physical Society, Petit-Lancy, 1998), p. 789.
[12]V. Antoni, L. Apolloni, M. Bagatin et al., in Plasma Physics and Controlled Nuclear Fusion 1994, in Proceedings of the 15th International Conference, Seville, 1994 (International Atomic Energy Agency, Vienna, 1995), Vol. 2, p. 405.
[13]Y. Yagi, H. Koguchi, H. Sakakita et al., Phys. Plasmas **6**, 3824 (1999).
[14]S. Martini, R. Piovan, P. Sonato et al., in Plasma Physics and Controlled Nuclear Fusion 1998, in Proceedings of the 17th International Conference, Yokohama, 1998 (International Atomic Energy Agency, Vienna, to be published).
[15]A. F. Almagri, S. Assadi, S. C. Prager et al., Phys. Fluids B **4**, 4080 (1992).
[16]D. J. Den Hartog, A. F. Almagri, J. T. Chapman et al., Phys. Plasmas **2**, 2281 (1995).
[17]A. K. Hansen, A. F. Almagri, D. J. Den Hartog, S. C. Prager, and J. S. Sarff, Phys. Plasmas **5**, 2942 (1998).
[18]R. Fitzpatrick, Phys. Plasmas **5**, 3325 (1998).
[19]R. Fitzpatrick, S. C. Guo, D. J. Den Hartog, and C. C. Hegna, Phys. Plasmas **6**, 3878 (1999).
[20]The standard large aspect-ratio ordering is $R_0/a \gg 1$, where R_0 and a are the major and minor radii of the plasma, respectively.
[21]The conventional definition of this parameter is $\beta = 2\mu_0\langle p\rangle/\langle B^2\rangle$, where $\langle\cdots\rangle$ denotes a volume average, p is the plasma pressure, and B is the magnetic field-strength.

[22]W. A. Newcomb, Ann. Phys. (N.Y.) **10**, 232 (1960).

[23]H. P. Furth, J. Killeen, and M. N. Rosenbluth, Phys. Fluids **6**, 459 (1963).

[24]R. Fitzpatrick, Nucl. Fusion **33**, 1049 (1993).

[25]A. F. Almagri, J. T. Chapman, C. S. Chiang *et al.*, Phys. Plasmas **5**, 3982 (1998).

[26]A. I. Smolyakov, A. Hirose, E. Lazzaro, G. B. Re, and J. D. Callen, Phys. Plasmas **2**, 1581 (1995).

[27]R. M. Coelho, E. Lazzaro, M. F. Nave, and F. Serra, Phys. Plasmas **6**, 1194 (1999).

[28]M. F. F. Nave and J. A. Wesson, Nucl. Fusion **30**, 2575 (1990).

[29]R. L. La Haye, T. H. Osborne, C. L. Rettig, C. M. Greenfield, A. W. Hyatt, and J. T. Scoville, Nucl. Fusion **8**, 988 (1995).

[30]L. L. Lao, R. J. La Haye, K. H. Burrell *et al.*, Phys. Plasmas **5**, 1050 (1998).

[31]J. M. Finn and C. R. Sovinec, Phys. Plasmas **5**, 461 (1998).

[32]T. H. Stix, Phys. Fluids **16**, 1260 (1973).

[33]A. H. Boozer, Phys. Fluids **24**, 1387 (1981).

[34]T. H. Jensen and M. S. Chu, J. Plasma Phys. **30**, 57 (1983).

[35]P. H. Rutherford, in *Basic Physical Processes of Toroidal Fusion Plasmas*, in *Proceedings of the Course and Workshop*, Varrena, 1985 (Commission of the European Communities, Brussels, 1986), Vol. 2, p. 531.

[36]M. Persson and A. Bondeson, Nucl. Fusion **29**, 989 (1989).

[37]T. C. Hender, C. G. Gimblett, and D. C. Robinson, Nucl. Fusion **29**, 1279 (1989).

[38]G. Berge, L. K. Sandal, and J. A. Wesson, Phys. Scr. **40**, 173 (1989).

[39]D. Edery and A. Samain, Plasma Phys. Controlled Nucl. Fusion Res. **32**, 93 (1990).

[40]H. Zohm, A. Kallenbach, H. Bruhns, G. Fussmann, and O. Klüber, Europhys. Lett. **11**, 745 (1990).

[41]T. H. Jensen, A. W. Leonard, R. J. La Haye, and M. S. Chu, Phys. Fluids B **3**, 1650 (1991).

[42]G. Kurita, T. Tuda, M. Azumi, and T. Takeda, Nucl. Fusion **11**, 1899 (1992).

[43]R. D. Parker, in *Controlled Fusion and Plasma Physics*, in *Proceedings of the 19th European Conference*, Innsbruck, 1992 (European Physical Society, Petit-Lancy, 1992), Vol. I, p. 427.

[44]R. Fitzpatrick, Phys. Plasmas **5**, 3325 (1998).

[45]D. A. Gates and T. C. Hender, Nucl. Fusion **36**, 273 (1996).

[46]G. A. Navratil, C. Cates, M. E. Mauel *et al.*, Phys. Plasmas **5**, 1855 (1998).

[47]W. A. Craven and A. J. Wootton, Nucl. Fusion **38**, 585 (1998).